Structure and superconductivity in pyrite $Ir_{0.95-x}Rh_xTe_2$: A comparison with analogous selenides

Jiangang Guo,[1,*] Yanpeng Qi,[1] and Hideo Hosono[1,2]

[1]*Frontier research center, Tokyo Institute of Technology, 4259 Nagatsuta-cho, Midori-ku, Yokohama 226-8503, Japan*

[2]*Materials and Structures Laboratory, Tokyo Institute of Technology, 4259 Nagatsuta-cho, Midori-ku, Yokohama 226-8503, Japan*

(Received 9 May 2013; published 11 June 2013)

We report the structural and superconducting evolution of the solid solution of $Ir_{0.95-x}Rh_xTe_2$ ($0 \leqslant x \leqslant 0.52$) and compare the results with those of analogous selenides. The structural analysis revealed that the unit cell unexpectedly expands and the separation of the Te_2^{-2} dimer exhibits a maximal value of around $x = 0.2$ with increasing Rh content. However, unlike the domed T_c in $Ir_{0.94-x}Rh_xTe_2$, the present system exhibits a monotonous decrease in T_c, which is independent of the instability of the Te_2^{-2} dimer. As the analysis of resistivity and heat capacity, it is suggested that electron-electron/phonon correlation strength is a considerable factor leading to the different evolution of T_c in the vicinity of the structural instability state of pyrite superconductors.

DOI: 10.1103/PhysRevB.87.224504 PACS number(s): 74.70.Xa, 74.70.Dd, 74.20.Mn

I. INTRODUCTION

Improving our understanding of the ground state of compounds that contain a heavy transition metal (TM) element has become increasingly desirable due to fascinating properties such as Mott insulator,[1,2] superconductivity,[3] and spin-orbital coupling.[4–6] Compared with the spatial extension (W) of the orbital of a $3d$ TM element, that of $4d/5d$ electron orbitals should be broader and there should be reduced on-site Coulomb repulsion (U). It is known that the group 9 K_2NiF_4-type oxides exhibit various intrinsic states, e.g., Sr_2CoO_4 is a ferromagnetic metal, whereas Sr_2RhO_4 is a simple metal.[7,8] The analogous $5d$-Sr_2IrO_4 is a Mott insulator, and the inherently different ground state could be ascribed to the nontrivial spin-orbital coupling (SOC) induced by the large crystal field effect.[4,6]

We have previously reported the exotic properties of defective $5d$-TM pyrite chalcogenides $Ir_{0.75}Ch_2$ (Ch = Se, Te), of which $Ir_{0.75}Se_2$ shows localized insulator behavior.[9] As Ir vacancies are gradually filled by Ir, the unit cell size and the separation of the Se_2^{-2} dimer systemically increases. Simultaneously, the transition from insulator to superconductor occurs, and the superconducting transition temperature (T_c) monotonically increases to 6.4 K. Furthermore, the $4d$ element Rh substitution for Ir leads to the unexpected expansion of the unit cell and the maximal separation of the Se_2^{-2} dimer. The compound $Ir_{0.58}Rh_{0.36}Se_2$ shows the highest T_c, 9.6 K, which corresponds to the weakest bonding state of the Se_2^{-2} dimer.[10] Meanwhile, the maximal T_c and the strongest electron-phonon coupling (EPC) emerge in the vicinity of the largest separation of the Se_2^{-2} dimer, which might be correlated with structural instability due to the destabilization of the anion dimers.

The analogous $Ir_{0.75}Te_2$ also could be synthesized at ambient pressure. This material is a metal at the weak-localized state and exhibits superconductivity at 1.8 K.[11] We thought pressure synthesis would be effective to increase the occupancy of Ir and further to stabilize the pyrite phase.[12] As a consequence, the maximal content of Ir could be enhanced to 0.93 for $Ir_{0.93}Te_2$ having the highest T_c of 4.7 K.[9] The variation of crystallographic parameters and T_c show similar features to those of the selenides. Nevertheless, the EPC strength of pyrite $Ir_{0.93}Te_2$, judging from the relatively smaller normalized heat-capacity jump, is clearly weaker than that of $Ir_{0.91}Se_2$.[9,10] It would therefore be of interest to elucidate how crystal structure and superconductivity evolve with $4d$ Rh metal substitution in reduced correlated pyrite $IrTe_2$ superconductors.

In this paper, we report the synthesis, structural changes, and superconducting properties of solid-solution $Ir_{0.95-x}Rh_xTe_2$ ($0 \leqslant x \leqslant 0.52$). The structural analyses indicated that the unit cell continuously expands and the separation of the Te_2^{-2} dimer had a maximum value at the intermediate composition. In contrast to that of $Ir_{0.94-x}Rh_xSe_2$, the T_c is just suppressed and appears to be irrelevant to the destabilization of the anion Te_2^{-2} dimer. Combined with the heat capacity analysis, the absence of a peak T_c in the range of the weakest bonding state of the dimer can likely be ascribed to the smaller electron-electron correlated strength of $Ir_{0.95-x}Rh_xTe_2$.

II. EXPERIMENT

Highly pure powders of Ir, Rh, and Te were mixed at the desired ratio, pelletized, and placed in an h-BN capsule. The assembly was heated at 1573 K and subjected to 5 GPa for 2 h using a belt-type high-pressure and high-temperature apparatus. All starting materials and precursors for the synthesis were prepared in a glove box filled with purified Ar gas (H_2O, $O_2 < 1$ ppm). The phase identification of the resulting samples was carried out by powder x-ray diffraction (PXRD) using a Bruker diffractometer (model D8 ADVANCE; Cu rotating anode). The Rietveld refinement of the PXRD patterns was performed using the TOPAS code.[13] Elemental compositions were determined using an electron-probe microanalyzer (EPMA, JEOL, Inc., model JXA-8530F). The micrometer scale compositions within the main phase were probed on 5 to 10 focal points, and the results were averaged. The dependence of dc electrical resistivity was measured by the conventional four-probe method with a physical property measurement system (PPMS, Quantum Design). Magnetic measurements were performed using a vibrating sample magnetometer (VSM, Quantum Design). Specific heat data were obtained using the conventional thermal relaxation method with the PPMS.

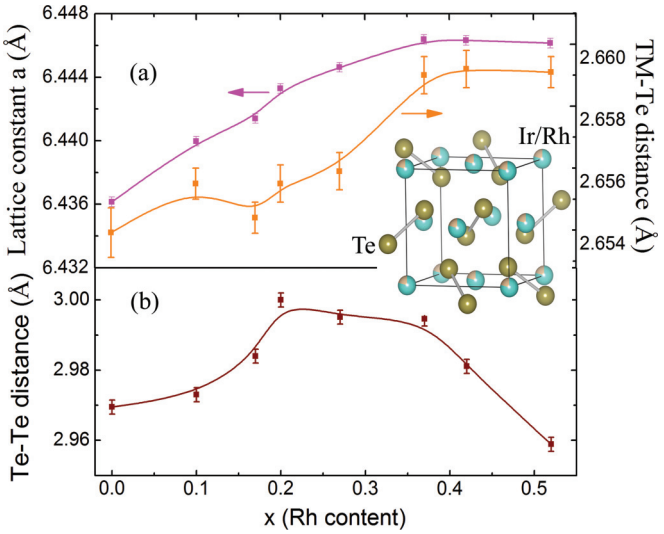

FIG. 1. (Color online) Crystal structure and sketched crystal structure of $Ir_{0.95-x}Rh_xTe_2$. (a), (b) The variation of lattice constants, the TM (Ir/Rh) -Te bond length, and the separation of the Te_2^{2-} dimer with increasing Rh content. The solid lines provide guides for orientation. Inset is the crystal structure of the $Ir_{0.95-x}Rh_xTe_2$ solid-state solution. The Oliver bonds denote the bonds of the Te-Te dimer.

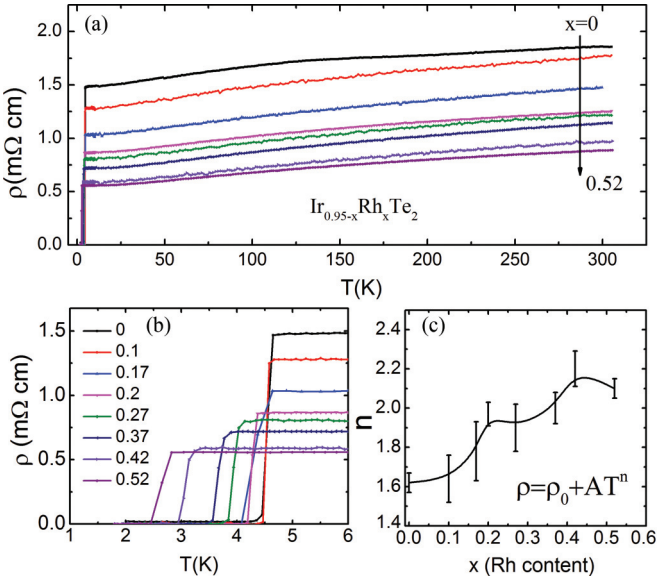

FIG. 2. (Color online) (a), (b) Temperature dependence of electrical resistivity under a zero magnetic field below 305 K and 6 K, respectively. (c) The value of n obtained from the fitting results of normal-state electrical resistivity up to 50 K.

III. RESULTS AND DISCUSSION

The EPMA results revealed that the sum of Ir and Rh is 0.95 ± 0.01, and thus the formation of vacancies can be negligibly small. The x-ray diffraction patterns of solid solutions could be successfully refined as a pyrite $IrTe_2$ model. The selected crystallographic parameters of $Ir_{0.95-x}Rh_xTe_2$ and the sketched crystal structure are shown in Fig. 1. As seen in Fig. 1(a), the lattice constant and Ir/Rh-Se bond length varied with increasing Rh content. Although the larger Ir^{4+} ions were substituted by smaller $4d$ Rh^{4+} ions, the size of the unit cell increased and then slowly saturated. The maximal lattice constant, 6.4462(3) Å, finally approached the reported value of $RhTe_2$.[14] As regards the separation of the Te_2^{-2} dimer, the value of 2.9695(2) Å initially increased, after which it decreased. The maximal distance between dimers emerged at about $x = 0.2$, which indicated that the bonding state of the Te_2^{-2} dimer was at its weakest state and exhibited a behavior similar to that of $Ir_{0.95-x}Rh_xSe_2$ (see below). Meanwhile, the Ir/Rh-Se bond length showed a similar trend in terms of the variation of the unit cell. The anomaly observed in the intermediate composition suggested that the Ir/Rh-Te bond is strongly affected by the weak bonding state of the Te_2^{-2} dimer. This complex structural change indicated that the dominant factor in lattice variation may not be the size of the transition element, but rather the geometry and polarization of the $TMCh_6$ polyhedral in a pyrite structure.[15]

Figure 2 shows the electrical transport properties of $Ir_{0.95-x}Rh_xTe_2$ from 2 to 300 K. As shown in Fig. 2(a), all samples exhibited metallic behavior, and the small hump observed at moderate temperatures quickly disappeared upon substitution of Rh for Ir. It is reported that a hump at 350 K for $Ir_{0.75}Te_2$ was identified as the structural transition from cubic lattice to rhombohedral lattice, which in general changed the distortion of the $IrTe_6$ polyhedra.[11] Provided that two types of humps have the same origin, it seems that Ir-filled and Rh doping could suppress the phase transition, which might be involved with the larger distortion of $IrTe_6$ polyhedral geometry and the enhanced charge fluctuation.[9] Within the lower temperature range, the resistivity of all samples suddenly decreased to zero. The detailed superconducting transition is shown in Fig. 2(b). The T_c monotonously decreased with increasing Rh content, and the lowest T_c under the present limitations was 2.4 K for $Ir_{0.43}Rh_{0.52}Te_2$. The interpolated T_c of $RhTe_2$ was 1.3 K, i.e., almost consistent with the reported value of 1.5 K.[14] In addition, the power-law equation $\rho = \rho_0 + AT^n$, where ρ_0 is residual resistivity and A is constant, could be applied to fit the normal-state resistivity below 50 K. The rhodium composition dependence of the obtained value n is plotted in Fig. 2(c). The value of n increased from 1.6 to 2 for $x = 0.2$, which indicated that the system might evolve into a Fermi-liquid metal. As $x > 0.2$, the normal-state resistivity behavior did not show any distinct changes. It should be noted that Fermi-liquid behavior emerged at $x = 0.2$, precisely where the separation of the Te_2^{-2} dimer also exhibited the largest value. In contrast to the domed T_c and T-linear resistivity in $Ir_{0.94-x}Rh_xSe_2$, the present superconducting properties displayed differing Rh-substitution dependency, in spite of the fact that both systems possess similar crystallographic properties.

The magnetic properties and specific heat (SH) at low temperatures are shown in Fig. 3. The upper panel reveals that there were large diamagnetic signals, indicating the bulk superconductivity nature for all samples. We can see that the T_c monotonously decreases as Rh substitution increases. The presence of hysteresis between zero field cooling and field cooling indicates that the materials are type-II superconductors. The lower panel shows the SH data for selected samples with values of $x = 0.2$, 0.27, and 0.42 plotted as

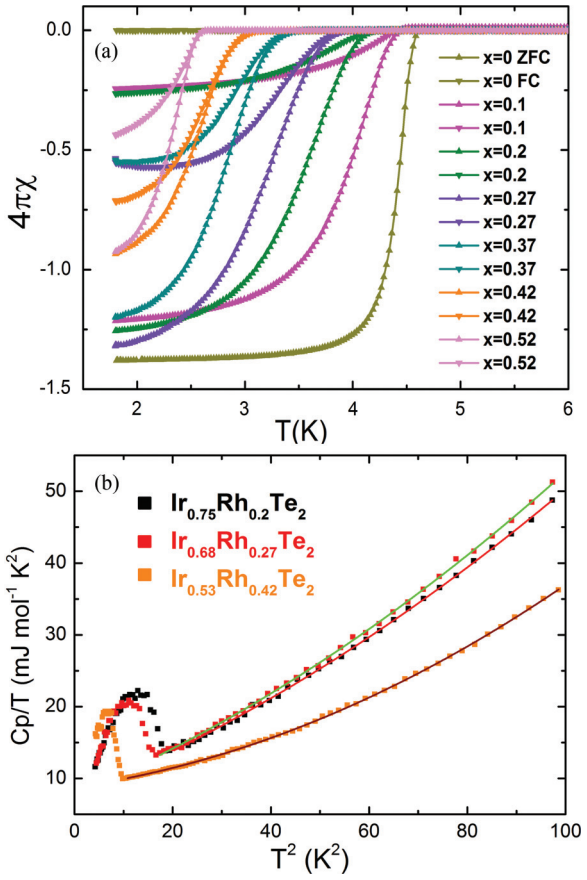

FIG. 3. (Color online) (a) Temperature dependences of magnetic properties at a magnetic field H of 10 Oe for $Ir_{0.95-x}Rh_xTe_2$. The upward and downward pointing triangles denote the zero-field-cooling (ZFC) and field-cooling (FC) process, respectively. (b) The total heat capacity divided by T as a function of temperature squared for $x = 0.2$, 027, and 0.42 at $H = 0$ KOe. The solid lines are the fitting results, shown as a modified Debye model (see text).

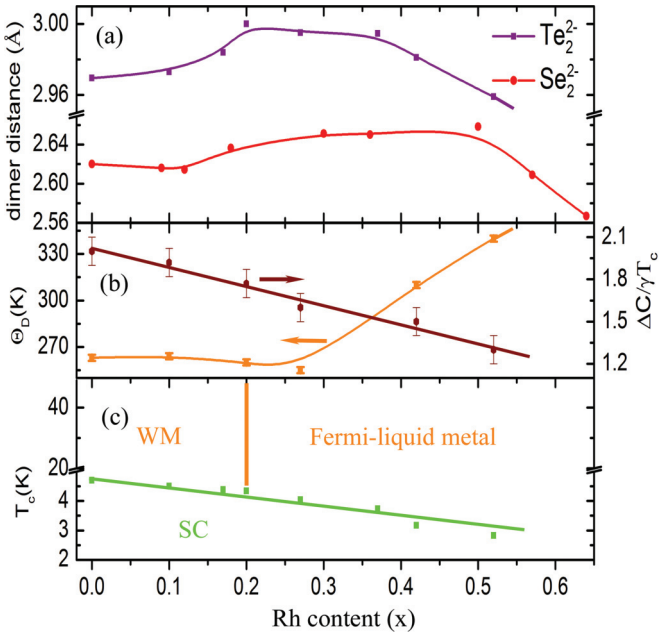

FIG. 4. (Color online) Summary and electronic phase diagram of $Ir_{0.95-x}Rh_xTe_2$. (a) The bond length of the anion Te-Te dimer depends on the content of Rh. The separation of Se-Se dimer is drawn as the reported data in Ref. 10. (b) The Debye temperature Θ_D and $\Delta C/\gamma T_c$ as a function of rhodium content x. (c) The electronic phase diagram of $Ir_{0.95-x}Rh_xTe_2$. The orange solid line denotes the crossover temperature from the weak-metal (WM) to the Fermi-liquid metal state. The solid lines are guides.

C_p/T versus T^2. Here, the temperature associated with the distinct jump in C_p/T coincided with the electrical and magnetic data. The SH data in the low-temperature range could be well fitted by $C_p/T = \gamma + \beta T^2 + \delta T^4$, which in turn means that the influence of high frequency acoustic phonon branches is more significant than those of selenides. The fitted curves yielded the Sommerfeld electronic coefficients $\gamma = 7.66$, 7.79, and 8.77 mJ/mol K^2 for $x = 0.2$, 0.27, and 0.42, respectively, which showed only slight increments in the samples with higher T_c. The Debye temperatures calculated from the equation $\Theta_D = (12\pi^4 nR/5\beta)^{1/3}$, where n is the number of atoms per formula unit and R is the gas constant, were 260, 257, and 330 K for three samples, respectively. Referring to the Θ_D (263 K) for $IrTe_2$, the present variation in the Debye temperature Θ_D was similar to that of $Ir_{0.94-x}Rh_xSe_2$. In other words, with lower-content Rh substitution, the Debye temperature changed slightly and reached the smallest value for $Ir_{0.68}Rh_{0.27}Te_2$ when the bonding of the Te_2^{2-} dimer was weakest. With higher Rh contents, the Debye temperature markedly increased once again. It was also noted that the normalized heat capacity jumped at T_c, $\Delta C/\gamma T_c$, and monotonously decreased from 2 to 1.3 for $Ir_{0.53}Rh_{0.42}Te_2$, which implies that the EPC strength transits from an intermediate to a weak coupling state. As previously reported, at the weakest bonding state of the Se_2^{2-} dimer, the peak value of $\Delta C/\gamma T_c$ was 3.53 and T-linear resistivity appeared, thus indicating stronger EPC and electron-electron correlation strength in the selenide system than in the present telluride system.[10]

The composition dependencies of the calculated Debye temperature and superconducting parameters are summarized in Fig. 4. Interestingly, the EPC state appeared to exhibit behavior similar to that of the decreasing T_c. Likewise, the larger γ in the lower-T_c sample is also unusual, and it implies that EPC strength governs the T_c and EPC strength decreases with increasing Rh content. Moreover, this consistency has also been reported in the analogous $Ir_{0.94-x}Rh_xSe_2$. Actually, density functional theory (DFT) and phonon spectrum calculations on tellurium[16] and $BaSi_2$[17] have pointed out that the increase in T_c is closely correlated with an enhancement of EPC strength due to the emergence of the soft phonon mode.

In addition, the smallest value of Θ_D emerges at the weakest bonding state of Te_2^{2-} dimers, which has been observed in $BaNi_2(Ge_{1-x}P_x)$ systems.[18] Such critical behavior usually implies phonon softening within the range of structural instability or transition.[18,19] However, there seems to be a lack of rigid correspondence between the critical nature of the separation of the anion dimer, Θ_D and T_c. Taking into account the competition of Hubbard repulsion U and the SOC scenario presented by Pesin and Belents,[5] we considered that the parent $Ir_{0.75}Se_2$ locates the boundary of the Mott insulator

phase, while $Ir_{0.75}Te_2$ would cross into the metal regime, due to the reduced U, provided the SOC does not change substantially. Based on previous DFT calculations of selenide, the Fermi energy is dominated by the strong hybridization of the Ir/Rh-d and Se-4p orbitals.[9,10] Therefore, the more spatially spread Te 5p orbital could increase the bandwidth and weaken the electron-electron correlation in $Ir_{0.95-x}Rh_xTe_2$, as reflected by the conventional Fermi-liquid metallic behavior and reduced EPC in the intermediate composition. Although the softest phonon mode may emerge in the range of the weakest bonding of Te_2^{2-} dimers, the relative smaller EPC may still not suffice to induce a peak T_c in weakly metallic telluride superconductors.

Here, we investigated the structural and superconducting properties of solid solutions of $Ir_{0.95-x}Rh_xTe_2$. Comparison study demonstrates that pyrite $IrCh_2$ (Ch = Se, Te) superconductors share common features with respect to structural changes and the destabilization of the Ch_2^{2-} dimer as Rh is substituted for Ir. However, the absence of a domed T_c implies that the degree of electron-electron correlation and EPC strength may be predominant comparing with the instability of the anion dimer in the evolution of superconductivity. Additional phonon spectrum calculations will be needed to clarify the contrasting behaviors of these systems.

ACKNOWLEDGMENT

This study was supported by the Funding Program for World-Leading Innovative R&D in Science and Technology, Japan.

*Author to whom correspondence should be addressed: guojg@lucid.msl.titech.ac.jp

[1]T. Mizokawa, L. H. Tjeng, G. A. Sawatzky, G. Ghiringhelli, O. Tjernberg, N. B. Brookes, H. Fukazawa, S. Nakatsuji, and Y. Maeno, Phys. Rev. Lett. **87**, 077202 (2001).

[2]H. Okabe, M. Isobe, E. Takayama-Muromachi, A. Koda, S. Takeshita, M. Hiraishi, M. Miyazaki, R. Kadono, Y. Miyake, and J. Akimitsu, Phys. Rev. B **83**, 155118 (2011).

[3]Y. Maeno, H. Hashimoto, K. Yoshida, S. Nishizaki, T. Fujita, J. G. Bednorz, and F. Lichtenberg, Nature (London) **372**, 532 (1994).

[4]B. J. Kim, H. Jin, S. J. Moon, J.-Y. Kim, B.-G. Park, C. S. Leem, J. Yu, T. W. Noh, C. Kim, S.-J. Oh, J.-H. Park, V. Durairaj, G. Cao, and E. Rotenberg, Phys. Rev. Lett. **101**, 076402 (2008).

[5]D. Pesin and L. Belents, Nature Phys. **6**, 376 (2010).

[6]B. J. Kim, H. Ohsumi, T. Komesu, S. Sakai, T. Morita, H. Takagi, and T. Arima, Science **323**, 1329 (2009).

[7]J. Matsuno, Y. Okimoto, Z. Fang, X. Z. Yu, Y. Matsui, N. Nagaosa, M. Kawasaki, and Y. Tokura, Phys. Rev. Lett. **93**, 167202 (2004).

[8]R. S. Perry, F. Baumberger, L. Balicas, N. Kikugawa, N. J. C. Ingle, A. Rost, J. F. Mercure, Y. Maeno, Z. X. Shen, and A. P. Mackenzie, New J. Phys. **8**, 175 (2006).

[9]Y. Qi, S. Matusishi, J. Guo, H. Mizoguchi, and H. Hosono, Phys. Rev. Lett. **107**, 217002 (2012).

[10]J. Guo, Y. Qi, S. Matusishi, and H. Hosono, J. Am. Chem. Soc. **134**, 20001 (2012).

[11]L. Li, T. F. Qi, L. S. Lin, X. X. Wu, X. T. Zhang, K. Butrouna, V. S. Cao, Y. H. Zhang, J. Hu, S. J. Yuan, P. Schlottmann, L. E. De Long, and G. Cao, Phys. Rev. B **87**, 174501 (2013).

[12]J. M. Léger, A. S. Pereira, J. Haines, S. Jobic, and R. Brec, J. Phys. Chem. Solids **61**, 27 (2000).

[13]TOPAS 2005, Version 3, Bruker AXS, Karlsruhe, Germany.

[14]S. Geller, J. Am. Chem. Soc. **77**, 2641 (1955).

[15]M. Birkholz and R. Rudert, Phys. Status Solidi B **245**, 1858 (2008).

[16]F. Mauri, O. Zakharov, S. de Gironcoli, S. G. Louie, and M. L. Cohen, Phys. Rev. Lett. **77**, 1151 (1996).

[17]J. A. Flores-Livas, R. Debord, S. Botti, A. S. Miguel, M. A. L. Marques, and S. Pailhes, Phys. Rev. Lett. **106**, 087002 (2011).

[18]D. Hirai, F. von Rohr, and R. J. Cava, Phys. Rev. B **86**, 100505(R) (2012).

[19]K. Kudo, M. Takasuga, Y. Okamoto, Z. Hiroi, and M. Nohara, Phys. Rev. Lett. **109**, 097002 (2012).